DOI: 10.3901/CJME.2014.01.001, available online at www.springerlink.com; www.cjmenet.com; www.cjmenet.com.cn

Review of Electronic Speckle Pattern Interferometry (ESPI) for Three Dimensional Displacement Measurement

YANG Lianxiang[1, 2, 3, *], XIE Xin[1], ZHU Lianqing[2], WU Sijin[2], and WANG Yonghong[3]

1 *Optical Laboratory, Department of Mechanical Engineering, Oakland University, Michigan 48309, USA*

2 *School of Instrument Science and Opto-Electronic Engineering, Beijing Information Science and Technology University, Beijing 100192, China*

3 *School of Instrument Science and Opto-Electronic Engineering, Hefei University of Technology, Hefei 230009, China*

Received April 1, 2013; revised October 9, 2013; accepted November 7, 2013

Abstract: Three dimensional(3D) displacements, which can be translated further into 3D strain, are key parameters for design, manufacturing and quality control. Using different optical setups, phase-shift methods, and algorithms, several different 3D electronic speckle pattern interferometry(ESPI) systems for displacement and strain measurements have been achieved and commercialized. This paper provides a review of the recent developments in ESPI systems for 3D displacement and strain measurement. After an overview of the fundamentals of ESPI theory, temporal phase-shift, and spatial phase-shift techniques, 3D deformation measurements by the temporal phase-shift ESPI system, which is suited well for static measurement, and by the spatial phase-shift ESPI system, which is particularly useful for dynamic measurement, are discussed. For each method, the basic theory, a brief derivation and different optical layouts are presented. The state of art application, potential and limitation of the ESPI systems are shown and demonstrated.

Keywords: electronic speckle pattern interferometry(ESPI), three dimensional displacement and strain measurement, static loading, dynamic loading, phase-shift technology

1 Introduction

Three dimensional(3D) displacements, which can be translated further into 3D strain and stress, are the key parameter for design, manufacturing and quality control. Due to rapid development of the manufacturing industry, especially for automobile and aerospace applications, rapid and optimization design concepts have already been widely accepted. These concepts all require the support of rapid and high sensitive measurement of 3D displacements[1–7].

The traditional technique for displacement and strain measurement is the resistance strain gauge method. Though it is still used by the industry due to its simplicity, it is a contact method which only provides point to point data. Results may be incorrect for an area where there is a strain concentration because of its low spatial resolution. Furthermore, the preparation of strain gauge measurement is time consuming. Therefore, advanced optical methods, due to their non-contact, full field characteristics, and high measurement sensitivity, have been widely accepted as displacement and strain measurement tool in industry[8–9]. Of these methods, electronic speckle pattern interferometry(ESPI) is the most sensitive and accurate method for full-field 3D displacement measurement[10–12].

ESPI measures displacement by evaluating the phase difference of two recorded speckle interferograms under different loading conditions. Combined with a phase shift technique, ESPI systems can measure the 3D displacement with dozens of nanometer level sensitivity. Cataloged by measurands, ESPI systems can be characterized as either out-of-plane, which measure the out-of-plane displacement w (displacement in the z-coordinate direction), or in-plane, which measures the in-plane displacement u (displacement in the x-coordinate direction) or v (displacement in the y-coordinate direction). For 3D measurement, all u, v, and w data are measured under a single loading. Different kinds of 3D measurement systems have been invented using different combinations of out-of-plane and in-plane setups. Cataloged by the phase extracting method, ESPI systems can be divided into fringe pattern ESPI systems, which were used in the early ages of ESPI, temporal phase shift ESPI systems, which are mainly suited for static or quasi static loading, and spatial phase-shift ESPI systems, which are suited well for dynamic loading[8–16]. By combining different measurands and phase extracting methods, a variety of ESPI systems exist for 3D displacement

* Corresponding author E-mail: yang2@oakland.edu

The project is supported by National Natural Science Foundation of China (Grant Nos. 51275054, 51075116)

measurement, and some of them have already been commercialized for real industry applications[16–18].

This paper provides a review of different approaches for 3D ESPI systems to measure 3D displacements. Section 2 provides an overview of the basic fundamentals of ESPI theory. Section 3 reviews the temporal phase-shift ESPI systems, which are the most widely used systems for 3D static displacement measurement. Section 4 discusses the spatial phase-shift ESPI system, which is specially designed for 3D dynamic displacement measurement. Basic theory and brief derivation are presented, and the potential capacities and limitations of ESPI systems for displacement measurement are discussed in detail.

2 Basic Principle of ESPI for Displacement Measurement

In optical interferometry, a phase difference is related to a displacement component. The fundamental of ESPI for measuring displacement components is to measure the relative phase difference between the object and reference beams[8]. This gives two key points of an ESPI system for displacement measurement: (1) Using different optical arrangements, ESPI systems can measure different displacement components; (2) Many technologies, through the use of a number of different phase evaluation algorithms, can be utilized to calculate the relative phase difference. A variety of ESPI systems have been invented and applied in real applications due to the combination of these two points[8–15].

In this section, the basic theory of ESPI is presented. First, a simple ESPI setup which measures out-of-plane displacement is discussed. Then an in-plane ESPI setup with two directional illuminations is shown. Finally, the fundamental configuration and theory for three dimensional displacement using ESPI are illustrated.

2.1 Out-of-plane displacement measurement using ESPI

Fig. 1 shows an ESPI setup for out-of-plane displacement measurement[8, 10]. A laser is split by a beam splitter into two beams: a reference beam and an object beam. The object beam goes through a beam expander to illuminate the object with an angle to the observation direction. The defused light reflected by the object is collected by a lens and imaged on the CCD camera. The reference beam is reflected by a cube beam splitter and reaches the CCD plane. The interference between the reference beam and object beam generates a speckle interferogram, also called a speckle pattern[8].

The object beam wave front and reference beam wave front can be expressed as follows:

$$U_o = a_o \exp(i\phi_o), \tag{1}$$

$$U_r = a_r \exp(i\phi_r), \tag{2}$$

where U_o and U_r represent the object beam wave front and reference beam wave front, and ϕ_o and ϕ_r represent the phase of the object beam and reference beam, respectively. The intensity of the speckle pattern recorded on the CCD camera can be written as

$$I = (U_o + U_r)(U_o + U_r)^* = a_o^2 + a_r^2 + 2a_o a_r \cos(\phi_o - \phi_r). \tag{3}$$

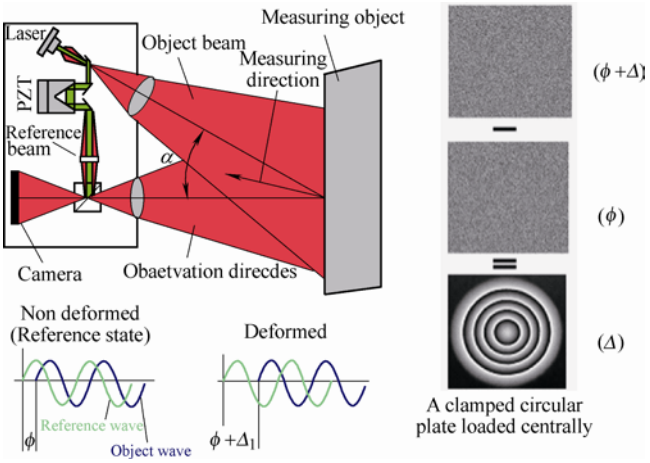

Fig. 1. ESPI setup for out-of-plane displacement measurement

The phase difference between the object beam and reference beam can be defined as $\theta = \phi_o - \phi_r$. Eq. (3) can be rewritten as

$$I = I_0(1 + \gamma \cos\theta), \tag{4}$$

where $I_0=(a_o^2+a_r^2)$ is the background and $\gamma = [2a_o a_r/(a_o^2+a_r^2)]$ is the contrast. After the object is deformed, the intensity recorded on the CCD camera becomes

$$I' = I_0[1 + \gamma \cos(\theta + \Delta)], \tag{5}$$

where Δ, which denotes the relative phase difference of the speckle patterns before and after loading, can be expressed as

$$\Delta = (\phi_o' - \phi_r') - (\phi_o - \phi_r) = (\phi_o' - \phi_o) - (\phi_r' - \phi_r) = \phi_o' - \phi_o, \tag{6}$$

where ϕ_o' and ϕ_r' represent the phase of the object beam and reference beam after loading. In the setup shown in Fig. 1, the phase difference of the reference bean $\phi_r' - \phi_r$ does not change due to the loading. Therefore, the relative phase difference Δ in this setup is equal to the phase difference of object beam $\phi_o' - \phi_o$.

The relative phase difference Δ results from a displacement caused by an applied loading. The relationship between the relative phase change Δ and displacement can be written as

$$\Delta = \frac{2\pi}{\lambda}\boldsymbol{d}\bullet\boldsymbol{s} = \frac{2\pi}{\lambda}(Au+Bv+Cw), \tag{7}$$

where $\boldsymbol{d}=(u, v, w)$ represents the displacement vector, where u and v are the in-plane components of the displacements in the x and y direction, respectively, and w is the out-of-plane component of the displacement. The sensitivity vector **s** can be expressed as $\boldsymbol{s}=(A, B, C)^{\mathrm{T}}=\boldsymbol{k}_{\mathrm{i}}-\boldsymbol{k}_{\mathrm{o}}$. Here, $\boldsymbol{k}_{\mathrm{i}}$ and $\boldsymbol{k}_{\mathrm{o}}$ are the unit vectors in the illumination and observation direction, respectively, and A, B, C are the sensitivity parameters. For the out-of-plane displacement measurement setup shown in Fig. 1, if the camera and the illumination source are located in the *xoz* plane and the angle between the illumination and the observation directions, known as illumination angle, is α, then the sensitivity vector $\boldsymbol{s}$ becomes $(\sin\alpha, 0, 1+\cos\alpha)^{\mathrm{T}}$. The relationship in Eq. (7) can then be expressed in Polynomial form:

$$\Delta=\frac{2\pi}{\lambda}[u\sin\alpha+w(1+\cos\alpha)]. \tag{8}$$

If the camera and illumination source are located in the *yoz* plane, then Eq. (8) becomes

$$\Delta=\frac{2\pi}{\lambda}[v\sin\alpha+w(1+\cos\alpha)]. \tag{9}$$

If α is set to zero, the relationship between the out-of-plane displacement and the relative phase difference Δ can be simplified as

$$\Delta=\frac{4\pi}{\lambda}w. \tag{10}$$

Eq. (10) shows that, with zero illumination angle in the optical arrangement shown in Fig. 1, the out-of-plane displacement can be directly evaluated by measuring the relative phase difference Δ in the speckle interferometry.

2.2 In-plane displacement measurement using ESPI

Fig. 2 shows a typical dual-beam ESPI setup for in-plane displacement measurement. Also known as a dual-beam illumination system, the two illumination beams illuminate the object symmetrically[14, 19, 21].

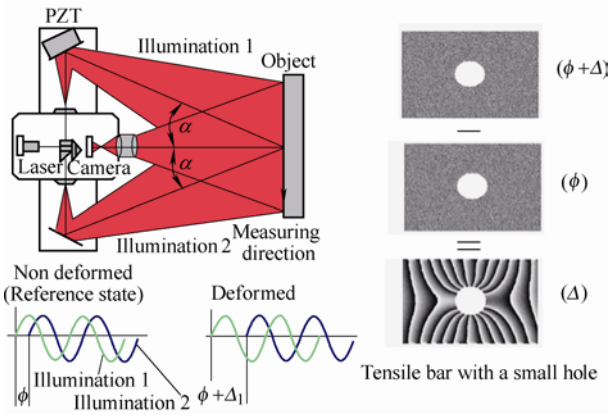

Fig. 2. Typical ESPI setup for in-plane displacement measurement

In this setup, the relative phase difference Δ shown in Eq. (6) becomes

$$\Delta=(\phi_1'-\phi_2')-(\phi_1-\phi_2)=\Delta_1-\Delta_2, \tag{11}$$

where ϕ_1, ϕ_2 and ϕ_1', ϕ_2' represent the phase of beam 1 and beam 2 before and after loading, respectively. For the setup shown in Fig. 2, assume the illumination angle is $+\alpha$ for beam 1, and the illumination angle for the beam 2 is $-\alpha$. Applying Eq. (8) for illumination beams 1 and 2, and assuming the laser source and CCD camera are located in the *XOZ* plane, the relative phase difference Δ of Eq. (11) becomes

$$\Delta=\Delta_1-\Delta_2=\frac{4\pi}{\lambda}(\sin\alpha)u. \tag{12}$$

If the laser source and CCD camera are oriented in the *YOZ* plane, the relative phase change can be written as

$$\Delta=\frac{4\pi}{\lambda}(\sin\alpha)v. \tag{13}$$

Eqs. (12) and (13) show that the in-plane displacement (u or v) can be directly evaluated by measuring the relative phase difference Δ of a dual-beam illumination ESPI System.

3 3D Displacement Measurement Using ESPI Systems for Static Loading

Eqs. (10), (12) and (13) show that the ESPI system is capable of determining both in-plane and out-of-plane displacements. The key point in determining these displacements is how to measure the relative phase difference Δ. In the early ages of ESPI, Δ was measured from direct subtraction of Eq. (4) from Eq. (5), which gives a fringe map. The phase difference can then be determined using the fringe orders. This is known as the fringe map approach. In this approach, the resolution for measuring phase difference is 2π. Later, this method was replaced by phase shift techniques, which increased the measurement sensitivity and resolution tenfold or more. Different phase shift techniques have been developed in the last two decades. They can be classified as two types: the temporal phase shift technique, which is mainly suited for static measurement, and the spatial phase shift technique, which is mainly suited for dynamic measurement. This section will review the temporal phase-shift technique for 3D displacement measurement. A 4+4 temporal phase shift technique is introduced, as it is the most commonly used algorithm in the temporal phase shift ESPI system. Then, three different approaches to achieve 3D displacement measurements are illustrated. Cataloged by different algorithms to determine the three displacement components,

these approaches are known as follows: (1) multiple out-of-plane setup approach[8, 6, 5], (2) out-of-plane and in-plane combined setup approach[8, 6, 7], (3) speckle pattern correlation approach[28–31].

3.1 Brief review of temporal phase shift technique

As mentioned above, measuring Δ is the key point to determining the displacement. Eqs. (4) and (5) show that there are three unknowns in the quantitatively recorded intensity equation, which are the background I_0, the contrast γ, and the phase distribution θ. Therefore, at least three linearly independent equations are needed to determine the phase distribution in Eq. (4) or Eq. (5). The temporal phase shift technique was developed to solve this problem[21–24]. Different research groups have developed several algorithms, such as 3+3, 4+4, 5+5, and N+N algorithms. However, the main idea of each algorithm is similar: to solve the phase distribution from multi intensity equations by recording multi-intensity images in a time series. Because multiple images are required at each loading condition, the technology is mainly suited for displacement measurement with a static loading.

Usually, a piezoelectric transducer(PZT) is utilized in ESPI setups as a phase shift component. A PZT can quickly move an accurate distance under a certain applied voltage. This enabled researchers to introduce a known phase shift to the optical path through step-by-step phase shifting and record multiple intensity maps with a given phase change. For example, for the most commonly used 4+4 temporal phase-shift algorithm, the PZT driver moves with a mirror in reference beam by four steps before loading, then moves another four steps after loading. For each step, the mirror moves a certain distance which corresponds to a phase change of $\pi/2$.

Before loading, four intensity maps are recorded by the four step phase shift:

$$\begin{cases} I_1 = I_0[1+\gamma\cos\ \theta], \\ I_2 = I_0\left[1+\gamma\cos\ \left(\theta+\dfrac{\pi}{2}\right)\right] = I_0[1-\gamma\sin\theta], \\ I_3 = I_0[1+\gamma\cos\ (\theta+\pi)] = I_0[1-\gamma\cos\theta], \\ I_4 = I_0\left[1+\gamma\cos\ \left(\theta+\dfrac{3\pi}{2}\right)\right] = I_0[1+\gamma\sin\theta], \end{cases} \tag{14}$$

where γ is the contrast, and θ is the phase difference between the object beam and reference beam.

Solving Eq. (14) for θ results in the following expression:

$$\theta\ (x,y) = \arctan\left(\frac{I_4-I_2}{I_1-I_3}\right). \tag{15}$$

In the same sense, four intensity maps I_1', I_2', I_3' and I_4' after loading are recorded and the corresponding phase difference θ' is given by

$$\theta'(x,y) = \arctan\left(\frac{I_4'-I_2'}{I_1'-I_3'}\right). \tag{16}$$

By subtracting Eq. (15) from Eq. (16) and considering that the phase differences are phase maps of modulus 2π, the relative phase difference due to a loading can be determined by Eqs. (17) and (18):

$$\Delta(x,y) = \theta'(x,y)-\theta(x,y)\ [\text{if}\ \theta'(x,y)>\theta(x,y)], \tag{17}$$

$$\Delta(x,y) = \theta'(x,y)-\theta(x,y)+2\pi\ (\text{if}\ \theta'(x,y)<\theta(x,y)). \tag{18}$$

Theoretically, for the temporal phase-shift technique, information from a 3 step phase shift is enough to evaluate the relative phase difference. However, the 4+4 temporal phase-shift algorithm is used more widely due to its simple calculation relationship, and the 5+5 algorithm is more accurate for the phase calculation.

The ESPI system's sensitivity increases tenfold or more by introducing a temporal phase-shift into the system. However, at the same time, the step shift also slows down the measurement speed, limiting its application mainly to static measurement. To overcome this disadvantage, several fast temporal phase shift algorithms, such as 4+1 and 3+1 algorithm, have been reported. However, those algorithms are all based on strong assumptions, such as the background and contrast of the speckle patterns before and after loading must be constant. The algorithms increase the measurement speed, but lower the phase map quality[18–20]. The most suitable approach to solving dynamic displacement problems is still the spatial phase shift method, which will be discussed in section 4.

3.2 Multiple out-of-plane setups approach

3.2.1 Three out-of-plane setup system

Eq. (7) shows a general relationship between the relative phase difference Δ and the displacements u, v, and w. A, B, and C are the sensitivity factors and can be determined if the positions of the lasers and camera are known. In this equation, only the relative phase difference Δ is known (determined either by the phase shift technique or fringe map approach), and u, v, and w are the three unknowns we want to determine. The most straight forward approach to solve for the 3 displacement components is to setup three ESPI setups with different illumination angles and one camera for observation. In combination with three switches, three speckle interferograms can be determined with different measurement sensitivity under a single loading. This approach was first reported by SHIBAYAMA K and UCHIYAMA H in 1971[25].

Fig. 3 shows the schematic of an ESPI system for 3D displacement measurement using three directional measuring systems. Each directional system uses an out-of-plane displacement measurement setup. An object

beam is used for illumination, and the reflected light meets with the reference beam in the image plane of the CCD camera.

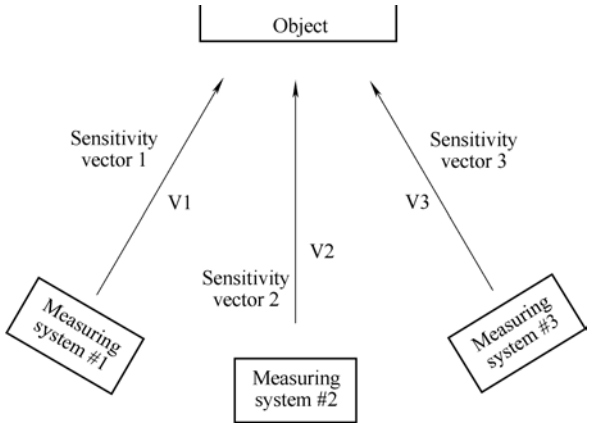

Fig. 3. 3D displacement measurement using three out-of-plane ESPI system

For each single illumination direction, one equation can be derived based on Eq. (7), resulting in a total of three linearly independent formulas:

$$\begin{aligned}\Delta_1 &= \frac{2\pi}{\lambda}\Delta L_g = \frac{2\pi}{\lambda}(A_1u+B_1v+C_1w),,\\ \Delta_2 &= \frac{2\pi}{\lambda}\Delta L_g = \frac{2\pi}{\lambda}(A_2u+B_2v+C_2w),\\ \Delta_3 &= \frac{2\pi}{\lambda}\Delta L_g = \frac{2\pi}{\lambda}(A_3u+B_3v+C_3w).\end{aligned} \tag{19}$$

Eq. (20) shows Eq. (19) in matrix form:

$$\begin{pmatrix}\Delta_1\\ \Delta_2\\ \Delta_3\end{pmatrix} = \frac{2\pi}{\lambda}\begin{pmatrix}A_1 & B_1 & C_1\\ A_2 & B_2 & C_2\\ A_3 & B_3 & C_3\end{pmatrix}\begin{pmatrix}u\\ v\\ w\end{pmatrix}. \tag{20}$$

The three displacement components u, v and w can be evaluated by solving Eq. (20):

$$\begin{pmatrix}u\\ v\\ w\end{pmatrix} = \frac{\lambda}{2\pi}\begin{pmatrix}A_1 & B_1 & C_1\\ A_2 & B_2 & C_2\\ A_3 & B_3 & C_3\end{pmatrix}^{-1}\begin{pmatrix}\Delta_1\\ \Delta_2\\ \Delta_3\end{pmatrix}. \tag{21}$$

This type of 3D displacement measurement system is the most straight forward way to measure 3D displacement using ESPI. However, due to the complexity of inverting matrices, it is not commonly used for 3D displacement measurement.

3.2.2 Four out-of-plane setup system

The four out-of-plane setup system utilizes four separate out-of-plane ESPI measurement setups. The four interferometers are arranged in special orientations, e.g., two are arranged left and right of the camera and the other two at up and down side of the camera with an equal but opposite illumination angle. Each illumination direction has its own reference beam, as shown in Fig. 4, to measure the 3D displacements.

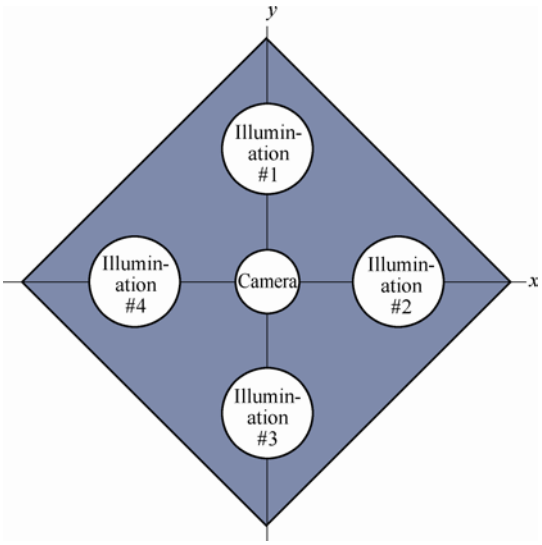

Fig. 4. Illumination arrangement for four out-of-plane setup

Applying Eqs. (8) and (9) to each single interferometer, an equation group can be obtained:

$$\Delta_1 = \frac{2\pi}{\lambda}\left[(\sin\alpha)v+(1+\cos\alpha)w\right],$$
for *yoz* illumination plane, top, (22a)

$$\Delta_2 = \frac{2\pi}{\lambda}\left[(\sin\alpha)u+(1+\cos\alpha)w\right],$$
for *xoz* illumination plane, right, (22b)

$$\Delta_3 = \frac{2\pi}{\lambda}\left\{[\sin(-\alpha)]v+[1+\cos(-\alpha)]w\right\},$$
for *yoz* illumination plane, bottom, (22c)

$$\Delta_4 = \frac{2\pi}{\lambda}\left[(\sin(-\alpha))u+(1+\cos(-\alpha))w\right].$$
for *xoz* illumination plane, left. (22d)

Through phase map subtraction and addition, the three displacement components u, v and w can be evaluated by

$$\Delta_1-\Delta_3 = \frac{4\pi}{\lambda}(\sin\alpha)v, \tag{23a}$$

$$\Delta_2-\Delta_4 = \frac{4\pi}{\lambda}(\sin\alpha)u, \tag{23b}$$

$$\Delta_1+\Delta_3 = \frac{4\pi}{\lambda}(1+\cos\alpha)w, \tag{23c}$$

$$\Delta_2+\Delta_4 = \frac{4\pi}{\lambda}(1+\cos\alpha)w. \tag{23d}$$

A commercial 3D Electronic Speckle Pattern Interferometer system, called Q-100, has been designed by Dantec Dynamics based on this theory. This system is miniaturized and can be attached to the testing object which can eliminate the influence of rigid body movement[8,13].

3.3 Out-of-plane and in-plane setup combined approach

A multiple Out-of-Plane setup approach described in 3.2 can solve a full 3D displacement problem by creating multiple directional phase maps, and evaluating the three displacement components *u*, *v* and *w* using phase map addition or subtraction operations described in Eq. (23). The disadvantage of this approach is that it is not a direct measurement for out-of-plane or in-plane displacements. As a result, the fringe pattern of in-plane or out-of-plane displacement cannot be observed directly during the loading or measurement. Therefore, a more direct 3D displacement measurement approach, known as an out-of-plane and in-plane setup combined approach, has been developed[8, 27]. This method utilizes two in-plane ESPI setups to measure the two in-plane displacements u and v, and one out-of-plane ESPI setup to measure the out-of-plane displacement[8, 27]. By utilizing an optical switch, the three measurement setup can be integrated together. The schematic of the setup is shown in Fig. 5.

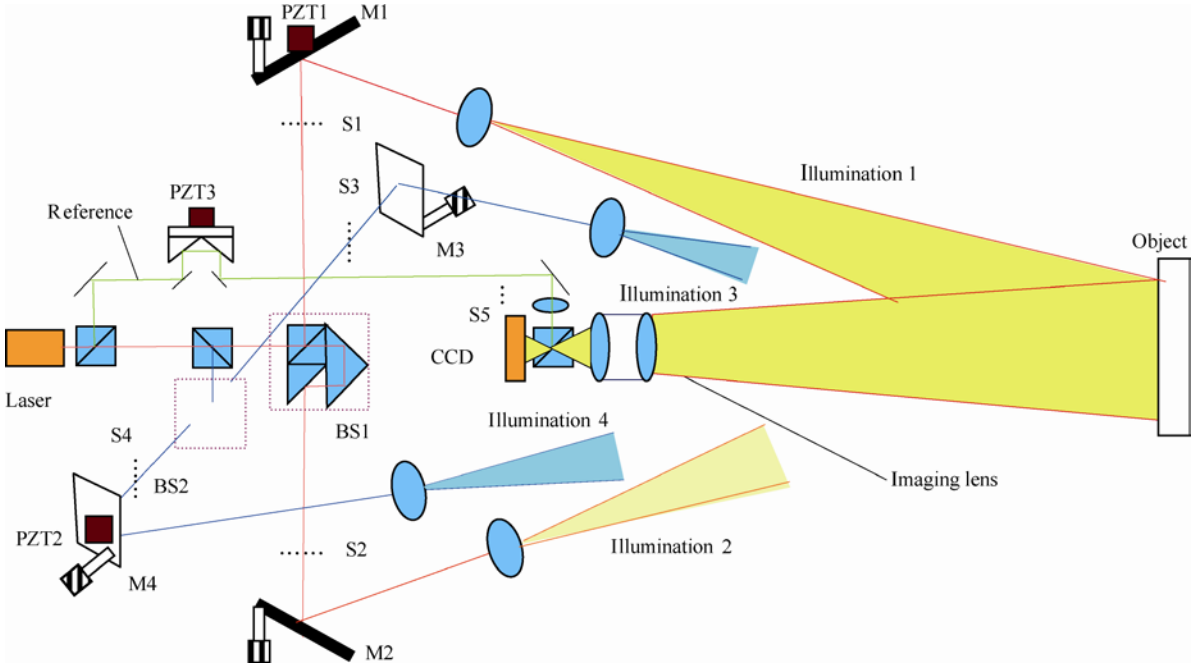

Fig. 5. Optical setup of out-of-plane and in-plane combined approach (BS: beam splitter; S: optical switcher)

As shown in Fig. 5, the laser is separated into five beams: illumination beams 1 and 2 are set in the *yoz* plane to measure *y*-direction in-plane displacement *v*. and illumination beams 3 and 4 are set in *xoz* plane to measure x-direction displacement *u*. Beam 5 serves as a reference beam and forms an out-of-plane interferometer by combining with illumination 3 or 4. The system can also use two lasers, one for illuminating beams 1, and 2, and the other for beams 3, 4 and 5. The system measures the in-plane displacement u by opening the optical switcher S_1 and S_2, while in-plane displacement *v* is measured by opening optical switcher S_3 and S_4. By opening one of the optical switchers of beams 3 and 4 and the reference beam 5, the system can measure the out-of-plane component *w*.

Based on Eqs. (12) and (13), the in-plane deformation *u* and *v* can be determined by

$$u = \Delta_1 \lambda / (4\pi \sin \alpha_1), \tag{24a}$$

$$v = \Delta_2 \lambda / (4\pi \sin \alpha_2), \tag{24b}$$

where Δ_1 and Δ_2 can be read directly from the phase map created by the temporal phase shift algorithm and α_n is the directional illumination angle, n=1, 2.

Using the measurement phase map created by the out-of-plane ESPI setup, the out-of-plane displacement can be determined based off of Eqs. (8) and (9):

$$w = \frac{\Delta_{\text{out}} \lambda - u \cdot (1 + \cos \alpha_{\text{out}}) \sin \alpha_{\text{out}}}{2\pi (1 + \cos \alpha_{\text{out}})}, \tag{25a}$$

$$w = \frac{\Delta_{\text{out}} \lambda - v \cdot (1 + \cos \alpha_{\text{out}}) \sin \alpha_{\text{out}}}{2\pi (1 + \cos \alpha_{\text{out}})}. \tag{25b}$$

where Δ_{out} is the phase determined by the phase map created from the out-of-plane ESPI system, and α_{out} is the illumination angle. The in-plane deformation *u* and *v* can be calculated from Eq. (24a) and Eq. (24b).

These three ESPI interferometers can be switched by order through the integration of an optical switch to the system. Because the in-plane ESPI setup and out-of-plane

setup measure the in-plane and out-of-plane displacement directly, there is no need to do further phase map operation, making real time phase map display possible (up to 2–3 Hz)[27].

This system has four illumination beams, two beams each in the horizontal and vertical direction to form an in-plane ESPI setup, which measures the in-plane displacement components u and v. By selecting one of those four beams as the illumination beam, combined with an inside build reference beam, an out-of-plane ESPI setup is formed which can measure the out-of-plane displacement directly.

3.4 Speckle pattern correlation approach

Besides the two illumination beam structured in-plane EPSI setup, another method exists to determine the in-plane displacement, known as electronic speckle photography or digital laser speckle correlation. This method determines the two in-plane displacement components through cross-correlation of corresponding sub-images. The correlation algorithm is purely mathematical, and is shown in detail in Refs. [28–31]. However, digital laser speckle correlation can only measure the in-plane displacement, so it cannot solve the full 3D displacement problem alone.

Ref. [24] provides an approach to solve the problem, which utilizes a typical out-of-plane ESPI setup. In this approach, the out-of-plane displacement is measured directly by the out-of-plane ESPI system using the temporal step phase shift technique. The in-plane displacement is calculated from the speckle pattern image using the digital laser speckle correlation algorithm. The out-of-plane displacement is measured from the phase-map, while the in-plane displacement is calculated from speckle pattern images. The sensitivity of the system for in-plane displacement, as a result, is lower than the out-of-plane displacement, reaching about $\lambda/10$. However, due to its simple optical structure, it is suitable for practical applications which do not have a high in-plane sensitivity requirement.

Recently, a three dimensional displacement measurement system, which purely uses the digital speckle correlation technique, has been reported in Ref. [29]. It still uses the conventional algorithm to calculate in-plane displacement with digital speckle photography. However, the out-of-plane displacement is not evaluated from out-of-plane ESPI. Instead, the out-of-plane displacement component is determined from the characteristic dependence of the speckle correlation on the spatial frequency. In this case, the system does not need a reference beam, resulting in an extremely simple setup consisting of a single camera with lens. However, as no phase shift technique is utilized, the measurement sensitivity is lower than the phase-shift ESPI system.

4 3D Displacement Measurement Using ESPI Systems for Dynamic Loading

The temporal phase-shift ESPI systems described in section 3 are usually suited for static or quasi-static measurement due to a requirement of multi images. For measurements under dynamic loading, spatial phase-shift ESPI systems are needed, because it is capable of evaluating a phase map from a single image[32–50].

The spatial phase shift technique can be divided into two catalogs: one known as the multichannel spatial phase-shift approach, and the other called the frequency carrier spatial phase shift method. The earlier approach to solve dynamical loading problem was to use multichannel spatial phase shift method[36–38]. Later, the frequency carrier method, a more advanced technique, was introduced. This method records multiple speckle interferograms on a single image. A Fourier transform method provides a way to extract and separate the each phase information from this single image. In this section, the multichannel spatial phase-shift approach will be introduced and the frequency carrier spatial phase shift method will be discussed in detail[41, 43–44].

4.1 Multiple channel spatial phase-shift approach

Temporal phase shift technique described above is to measure the phase distribution by recording multi-images (3 or 4 images) by a single camera in the time series. The Multiple channel spatial phase-shift approach is to record the 3 images (or 4 images or more) by three cameras (or 4 cameras or more) simultaneously and to generate a phase shift φ between those cameras. The phase distribution can then quickly be determined[36–38].

$$\begin{cases} I_1 = I_0(1+\gamma\cos\theta), \\ I_2 = I_0[1+\gamma\cos(\theta+\varphi)], \\ I_3 = I_0[1+\gamma\cos(\theta+2\varphi)], \end{cases} \tag{26a}$$

where φ is a phase shift between each camera. If the phase shift $\varphi = 2\pi/3$, the phase difference θ can be calculated by

$$\theta = \arctan\frac{\sqrt{3}(I_1 - I_3)}{2I_2 - I_1 - I_3}. \tag{26b}$$

However, the setup arrangement in the multi cameras system, especially the generation of the phase shift between those cameras, is practically hard to achieve, and the turbulence caused by relative position movement will generate great error in this system. The cost of this approach is also great, so there have been few real applications for this kind of approach. Later on, an alternative idea was introduced to determine phase distribution with a single image by using only a single CCD camera. In this method, each pixel likes a channel. Instead

of creating phase shift among each camera, this idea is to generate a spatial phase shift among three neighborhood pixels by adjusting the reference beam. Fig. 6 shows the schematic of the idea. By setting the reference beam an appropriate angle α, an optical path difference(OPD) between two adjacent pixels is created:

$$OPD = s \cdot \sin\alpha, \tag{27a}$$

where s is the pixel size. If a laser wavelength used is λ, a phase shift is obtained by

$$\varphi = (OPD/\lambda)\, 2\pi = (s \cdot \sin\alpha/\lambda)\, 2\pi. \tag{27b}$$

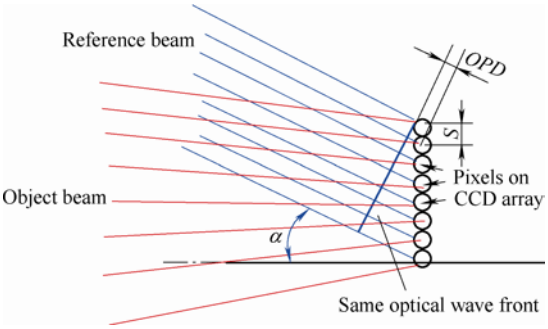

Fig. 6. Schematic of ESPI approach for generating a spatial phase shift among pixels

Using intensity data of three adjacent pixels, the phase distribution can be calculated as presented in Eq. (26)[37–38].

4.2 1D frequency carrier spatial phase-shift method

The multiple channel approach can determine phase distribution from a single speckle interferogram and, thus, it is suited for dynamic measurement. However, three or more pixels are needed to determine one point phase distribution which results in reducing the spatial resolution, and, thus, greatly influences the measurement accuracy. Additionally, this approach can only conduct one dimensional measurement, such as, the out-of-plane deformation measurement. To measure all three displacement components under a dynamic loading, three interferometers are needed and they must work simultaneously as well. To achieve this objective, a frequency carrier method must be introduced to measure multiple displacement components in one shot[39–41].

To better understand the 3D frequency carrier spatial phase-shift approach, a 1D frequency carrier method for out-of-plane displacement measurement will be introduced first. Fig. 7 shows the fundamental setup. The setup is similar to the conventional out-of-plane ESPI system, except that the reference beam is carried by an optical fiber and tilted with an arranged angle to illuminate the CCD plane. This special angle brings an additional spatial frequency into the reference beam. Utilizing this spatial frequency after the Fourier transform shifts the spectrums on the frequency domain. The spatial frequency also helps to separate the spectrums which contain the phase information of the recorded interferogram. After that, the phase information is filtered out by the Windowed Fourier inverse transform and evaluated.

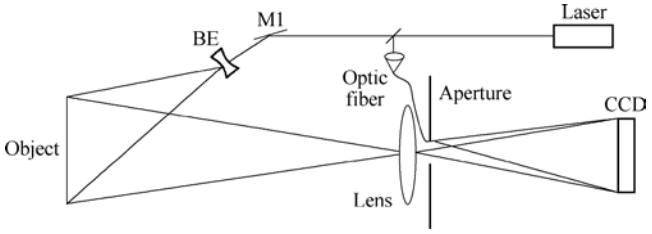

Fig. 7. Schematic of spatial phase-shift holography setup for Out-of-plane displacement measurement

The wave fronts from the object beam (u_1) and reference beam (u_2) can be written as follows:

$$u_1(x, y) = |u_1(x, y)| \exp[i\varphi(x, y)], \tag{28}$$

$$u_2(x, y) = |u_2(x, y)| \exp(-2\pi i f_{0x} \cdot x - 2\pi i f_{0y} \cdot y), \tag{29}$$

where $f_{0x} = (\sin\theta_{0x} / \lambda)$, $f_{0y} = (\sin\theta_{0y} / \lambda)$, θ_{0x} and θ_{0y} are the directional illumination angles of the reference beam, and λ is the wavelength of the laser.

The intensity recorded on the CCD camera can be expressed as follows:

$$I(x, y) = (u_1 + u_2) \cdot (u_1^* + u_2^*). \tag{30}$$

After Fourier transform,

$$FI = U_1^2 + U_2^2 + U_1(f_x, f_y) \otimes U_2(f_{0x}, f_{0y})^* + U_2(f_{0x}, f_{0y}) \otimes U_1(f_x, f_y)^*, \tag{31}$$

where $\otimes$ is the convolution operation, $U_1(f_x, f_y) = FT(u_1)$, $U_2(f_{0x}, f_{0y}) = FT(u_2)$.

Among the four terms in Eq. (31), $U_1^2 + U_2^2$ term, located at the center (f_x, f_y), is a low frequency term which mainly contains the background information. $U_1(f_x, f_y) \otimes U_2(f_{0x}, f_{0y})$ and $U_2(f_{0x}, f_{0x}) \otimes U_1(f_x, f_y)$ terms are conjugated terms, which are located at $(f_x - f_{0x}, f_y - f_{0y})$ and $(f_{0x} - f_x, f_{0y} - f_y)$ respectively. This is shown in Fig. 8.

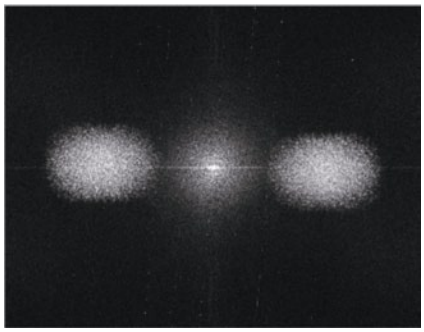

Fig. 8. Spectrum of speckle pattern image

By properly selecting an illumination angle for the reference beam and aperture size, the three spectrums on the Fourier domain can be separated, and, by properly selecting the windowed Fourier inverse transform(WIFT) and complex amplitude calculations, the phase difference can be calculated using Eq. (32),

$$\left[\varphi(x,y)+2\pi x f_{0x}+2\pi y f_{0y}\right]=\arctan\frac{\mathrm{Im}[u_2u_1^*]}{\mathrm{Re}[u_2u_1^*]}, \tag{32}$$

Im and Re denote the imaginary and real part of the complex numbers.

After displacement, the phase difference can be calculated using Eq. (33):

$$\left[\varphi'(x,y)+2\pi x f_{0x}+2\pi y f_{0y}\right]=\arctan\frac{\mathrm{Im}[u_2u_1^*]}{\mathrm{Re}[u_2u_1^*]}. \tag{33}$$

By subtraction, the out-of-plane displacement can be evaluated from the relative phase difference:

$$\Delta=\varphi-\varphi'=\frac{2\pi}{\lambda}(1+\cos\alpha)w, \tag{34}$$

where α is the illumination angle and w is the out-of-plane displacement. Because the illumination angle α is very small for out-of-plane measurement, it can be regarded as zero. As a result, the $(1+\cos\alpha)$ term equals one. Then Eq. (34) becomes a simple linear relationship, and the out-of-plane displacement can be evaluated by a simple linear relationship. Fig. 9 shows a typical phase map evaluated from the 1D frequency carrier spatial phase-shift ESPI system.

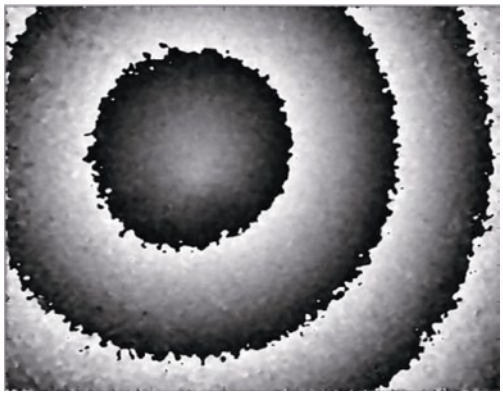

Fig. 9. Phase map of a shearogram corresponding to an out-of-plane displacement

4.3 3D frequency carrier spatial phase-shift ESPI system

In section 4.2, a method was introduced which utilizes one spatial frequency shift to separate one interferogram spectrum on the frequency domain. This method can also be used to separate multiple interferogram spectrums by utilizing multiple spatial frequency shifts[46–51].

Fig. 10 shows the experimental setup of a 3D spatial phase-shift ESPI system. Three 1D frequency carrier phase shift ESPI setups are integrated together to measure the object from three different directions simultaneously. Three lasers of different wave lengths are used to avoid interference between different measurement directions.

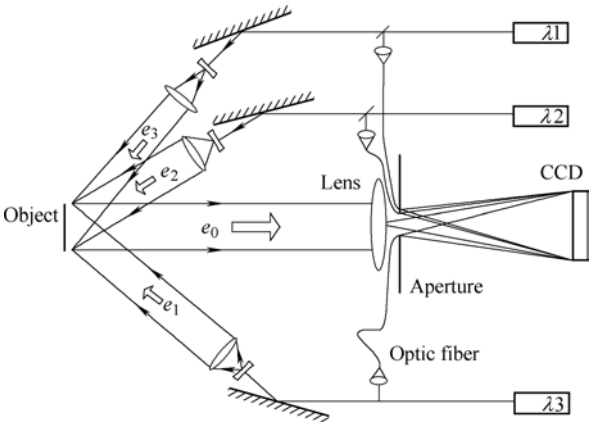

Fig. 10. Schematic of 3D spatial phase-shift holography measurement setup

The three reference beams are carried by optical fibers, each of them illuminating the CCD plane with a unique angle. In this case, three different frequency shifts are built into the three reference beam equations. Similarly with the 1D phase evaluation processing, one single speckle pattern image is transformed on the frequency domain by Fourier Transform.

Fig. 11 shows a spectrum of a speckle pattern image with three spatial frequency shifts. After Windowed Inverse Fourier Transform, three phase maps, corresponding to three directional measurements, are evaluated. The three evaluated phase maps can be further evaluated using Eq. (21) to calculate 3D displacement.

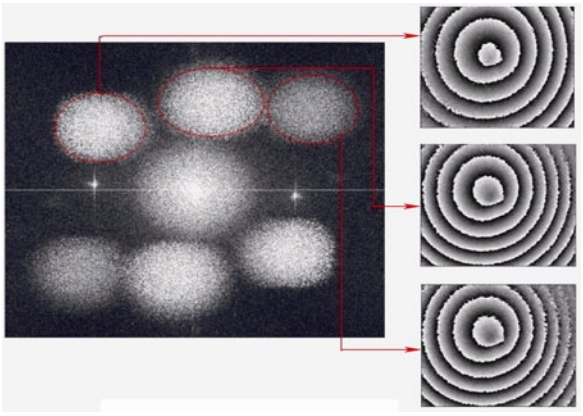

Fig. 11. Spectrum of speckle pattern image with three spatial frequency shift and evaluated phase maps

Using this algorithm, three dimensional displacements can be calculated from a single speckle pattern image. This greatly increases the measurement speed, enabling the measurement of simultaneous 3D displacement under dynamic loading. The image processing procedure is shown in Fig. 12.

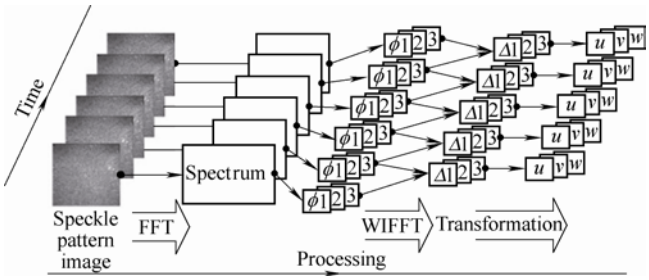

Fig. 12. Image processing of 3D displacement measurement system

This section discusses two types of spatial phase shift ESPI systems for 3D displacement measurement: Multiple Channel Spatial Phase-Shift ESPI system and frequency carrier spatial phase-shift ESPI system. However, in practice, the spatial phase shift technique can be combined with other phase evaluation techniques to form a hybrid measurement system. Ref. [45] is an example of this kind of system.

Both systems are pure spatial phase shift systems. Ref. [45] reported a 3D ESPI system which combined the 1D frequency carrier spatial phase-shift ESPI technique with the digital speckle correlation technique. The reported system uses the 1D frequency carrier spatial phase-shift ESPI method to evaluate out-of-plane displacement using a single speckle pattern image, and the digital speckle correlation algorithm to calculate the in-plane displacement.

5 Applications

This section provides a selection of three typical applications of the 3D ESPI system in the manufacturing, microelectromechanical systems (MEMS) and biomedical industry.

The 3D ESPI method is getting more and more acceptance in the manufacturing industry. It provides continuous full-field 3D displacement data, which can be easily transformed into strain by derivation. It is also suitable for the calibration, validation, and improvement of CAE models in the manufacturing industry.

A strain tensor is expressed as

$$\varepsilon = \begin{pmatrix} \dfrac{\partial u}{\partial x} & \dfrac{\partial v}{\partial x} & \dfrac{\partial w}{\partial x} \\ \dfrac{\partial u}{\partial y} & \dfrac{\partial v}{\partial y} & \dfrac{\partial w}{\partial y} \\ \dfrac{\partial u}{\partial z} & \dfrac{\partial v}{\partial z} & \dfrac{\partial w}{\partial z} \end{pmatrix}. \tag{35}$$

3D displacements $u(x, y)$, $v(x, y)$, and $w(x, y)$ can be determined from the measurement results of 3D ESPI. The 3D displacement measured is a function of x and y; thus the strains of the first two columns in the 3D strain tensor can be calculated by derivation[52]. The principle strain can also be determined using calculated strain components combined with the principles of Mohr's circle.

Fig. 13 shows a comparison between a 3D ESPI system (called Micro Star from a German Company) and the conventional strain gauge method for strain measurement of a composite component with a hole under a tensile stress. On the left of the hole, 4 resistance strain gauges were used to measure strains at four positions. At the same time, on the right of the hole, a 3D ESPI system was utilized to measure the full field strain. A comparison of the strain measurement results shows that the 3D ESPI system can measure full field strain with very high spatial resolution, while the conventional strain gauge can only measure the average and local strain over the gauge length. The curve demonstrates the strain distribution over a horizontal line on the right side and four points show the four strain gauge data on the left side. The original (zero position) of x-coordinate is the edge of the hole. Under a tensile stress, the strain distribution should be same or very close between left and right sides due to a symmetric relationship. The comparison shows that the strain data match well for the left three points, whereas, the strain at the leftmost strain gauge which is most close to the edge of the hole is much lower than the ESPI value because there was a strain concentration at the edge of hole and the strain was lowered due to an average function over the strain gauge area (about 2 mm×2 mm). It is obvious that ESPI has a high spatial resolution and provides more accurate data in the strain concentration area.

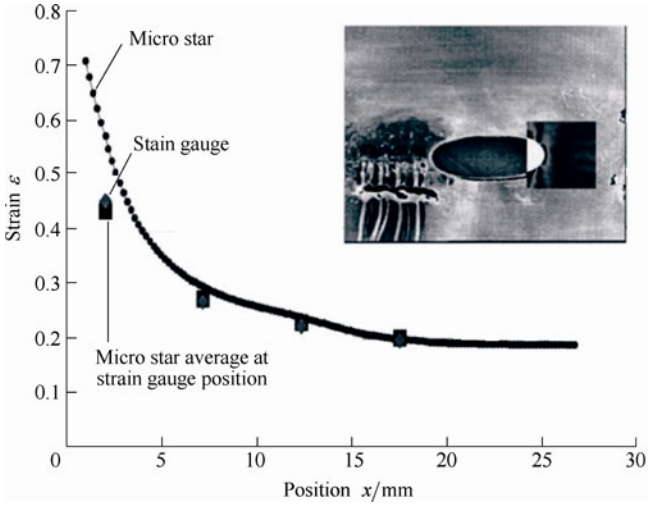

Fig. 13. 3D ESPI application for strain measurement around a hole area

Fig. 14 shows an application of measuring the motion of a MEMS mirror. The phase distributions before and after tilting the middle MEMS mirror are shown in Figs. 14(a) and (b). The phase difference between the two distributions gives the result in Fig. 14(c) showing the motion of the middle MEMS mirror induced by applying a voltage[53].

Another example of 3D ESPI application is in the biomedical area. Bone is a mechanosensitive tissue that adapts its mass, architecture and mechanical properties to

external loading. In this application, a 3D ESPI system is used to study the 3D displacement and strain behavior under applied loading[10].

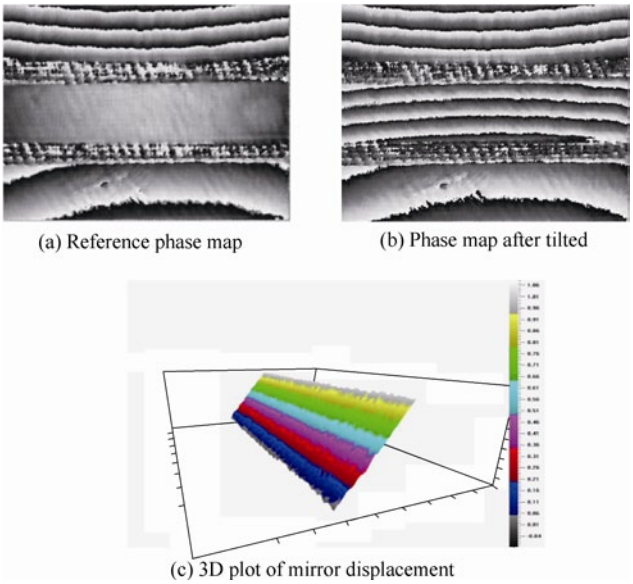

(a) Reference phase map (b) Phase map after tilted

(c) 3D plot of mirror displacement

Fig. 14. Displacement measurement for MEMS components

Fig. 15 shows the measured mice bone. The bone is fixed in one end and free in the other end. The mechanical loading is applied by computer controlled piezoelectric loading device. Fig. 16 shows the measured 3D displacement and calculated principle strain under 1N force loading.

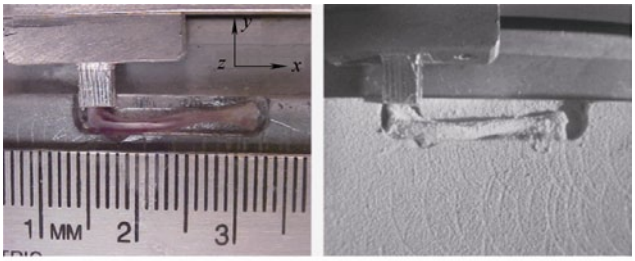

(a) Sample prior to white spray (b) Vample coated with white spray

Fig. 15. Mouse femur on a sample table

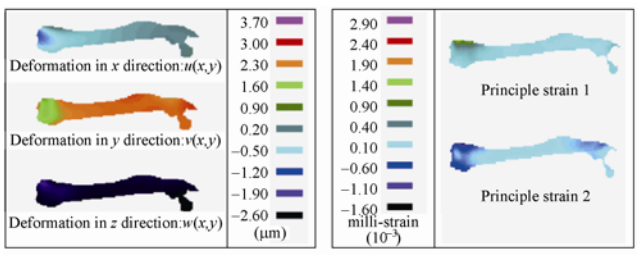

(a) 3D components of displacement (b) Calculated strains

Fig. 16. Microscopic displacements and strains on a femoral surface in response to 1N: ts

6 Conclusions

This paper reviews the ESPI technique for 3D displacement measurement. ESPI is a suitable optical measurement technique for 3D displacement and strain measurement. During the past decades, the ESPI method has received greater acceptance from the manufacturing industry for 3D displacement and strain measurement. It has also expanded its application into MEMS and biomedical industries. In the past decade, it has been developed from a 3D static measurement method into a 3D dynamic measurement method. It still has the potential for further exploration and applications.

Acknowledgments

The authors would also like to express their sincere thanks to Mr. SIA Bernard, a PhD candidate of *the Optical Laboratory at Oakland University*, who carefully and thoroughly read the manuscript and provide valuable criticisms.

References

[1] YANG L X, COLBOURNE P. Digital laser micro-interferometer and its applications[J]. *Optical Engineering*, 2003, 42(5): 1 417–1 426.

[2] OHLSSON R, WIHLBORG A, WESTHERG H. The accuracy of fast 3D topography measurements[J]. *International Journal of Machine Tools and Manufacture*, 2001, 41(13): 1 899–1 907.

[3] FU Yongqi, KOK N, BRYAN A. Microfabrication of microlens array by focused ion beam technology[J]. *Microelectronic Engineering*, 2000, 54(3): 211–221.

[4] GENSLER H M, MENG E. Rapid fabrication and characterization of MEMS Parylene C bellows for large deflection applications[J]. *Journal of Micromechanics and Microengineering*, 2012, 22(11): 115031.

[5] REMBE C, MULLER R S. Measurement system for full three-dimensional motion characterization of MEMS[J]. *Journal of Microelectromechanical Systems*, 2002, 11(5): 479–488.

[6] CHEN Xu, XU Nan, YANG L X, et al. High temperature displacement and strain measurement using a monochromatic light illuminated stereo digital image correlation system[J]. *Measurement Science and Technology*, 2012, 23(12): 125603

[7] WU SIJIN, HE Xiaoyuan, YANG L X. Enlarging the angle of view in Michelson-interferometer-based shearography by embedding a 4f system[J]. *Applied Optics*, 2011, 50(21): 3 789–3 794.

[8] YANG L X, ETTEMEYER A. Strain measurement by three-dimensional electronic speckle pattern interferometry: potentials, limitations, and applications[J]. *Optical Engineering*, 2003, 42(5): 1 257–1 266.

[9] CHEN Xu, YANG L X, XU Nan, et al. Cluster approach based multi-camera digital image correlation: Methodology and its application in large area high temperature measurement[J]. *Optics & Laser Technology*, 2013, http://dx.doi.org/10.1016/j.optlastec. 2013. 08.005.

[10] CHEN F, BROWN G M, SONG M. Overview of three-dimensional shape measurement using optical methods[J]. *Optical Engineering*, 2000, 39(1): 10–22.

[11] SCHNARS U, JUPTNER W P. Digital recording and numerical reconstruction of holograms[J]. *Measurement Science and Technology*, 2002, 13(9): R85.

[12] YANG L X, ZHANG Ping, LIU Sheng, et al. Measurement of strain distributions in mouse femora with 3D-digital speckle pattern interferometry[J]. *Optics and Lasers in Engineering*, 2007, 45(8): 843–851.

[13] XU Nan, XIE Xin, HARMON G, et al. Quality inspection of spot

welds using digital shearography[J]. *SAE International Journal of Materials & Manufacturing*, 2012, 5(1): 96–101.

[14] MOORE A J, TYRER J R. An electronic speckle pattern interferometer for complete in-plane displacement measurement[J]. *Measurement Science and Technology*, 1990, 1(10): 1 024.

[15] TONG Jingwei, ZHANG Dongsheng, LI Hongqi, et al. Study on in-plane displacement measurement under impact loading using digital speckle pattern interferometry[J]. *Optical Engineering*, 1996, 35(4): 1 080–1 083.

[16] DantecDynamics, ESPI-Q100[OL]. http://www. dantecdynamics. com/ Default.aspx?ID=853.

[17] Laser Technology Inc., Laser Shearography Technology[OL]. http://www.laserndt.com/technology/shearography.htm.

[18] ZHU Lianqing, WANG Yonghong, XU Nan, et al. Real-time monitoring of phase maps of digital shearography[J]. *Optical Engineering*, 2013, 52(10): 101902.

[19] SITOHI R S, BURKE J, HELMERS H, et al. Spatial phase shifting for pure in-plane displacement and displacement-derivative measurements in electronic speckle pattern interferometry (ESPI)[J]. *Applied optics*, 1997, 36(23): 5 787–5 791.

[20] ZHANG Jingbo. Two-dimensional in-plane electronic speckle pattern interferometer and its application to residual stress determination[J]. *Optical Engineering*, 1998, 37(8): 2 402–2 409.

[21] TAKEDA M, YAMAMOTO H. Fourier-transform speckle profilometry: three-dimensional shape measurements of diffuse objects with large height steps and/or spatially isolated surfaces[J]. *Applied Optics*, 1994, 33(34): 7 829–7 837.

[22] JOENATHAN C, FRANZE B, HAIBLE P, et al. Speckle interferometry with temporal phase evaluation for measuring large-object deformation[J]. *Applied Optics*, 1998, 37(13): 2 608–2 614.

[23] KAO C C, YEH G B, LEE S S, et al. Phase-shifting algorithms for electronic speckle pattern interferometry[J]. *Applied Optics*, 2002, 41(1): 46–54.

[24] WANG Liusheng, JAMBUNATHAN K, DOBBINS B N, et al. Measurement of three-dimensional surface shape and deformations using phase stepping speckle interferometry[J]. *Optical Engineering*, 1996, 35(8): 2 333–2 340.

[25] SHIBAYAMA K, UCHIYAMA H. Measurement of three-dimensional displacements by hologram interferometry[J]. *Applied Optics*, 1971, 10(9): 2 150–2 154.

[26] MARTINEZ A, RAYAS J A, RODRIGUEZ-VERA R, et al. Three-dimensional deformation measurement from the combination of in-plane and out-of-plane electronic speckle pattern interferometers[J]. *Applied optics*, 2004, 43(24): 4 652–4 658.

[27] Dantec Dynamics, ESPI-Q300[OL]. http://www.dantecdynamics. com/ Default.aspx?ID=854.

[28] SJODAHL M, SALDNER H O. Three-dimensional deformation field measurements with simultaneous TV holography and electronic speckle photography[J]. *Applied Optics*, 1997, 36(16): 3 645–3 648.

[29] FRICKE-BEGEMANN T. Three-dimensional deformation field measurement with digital speckle correlation[J]. *Applied Optics*, 2003, 42(34): 6 783–6 796.

[30] YAMAGUCHI I, FUJITA T. Linear and rotary encoders using electronic speckle correlation[J]. *Optical Engineering*, 1991, 30(12): 1 862–1 868.

[31] SEOKHO N, YAMAGUCHI I. Two-dimensional measurement of strain distribution by speckle correlation[J]. *Japanese Journal of Applied Physics*, 1992, 31(9A): 1 299–1 299.

[32] TAKEDA M, Gu Q, KINOSHITA M, TAKAI H, et al. Frequency-multiplex Fourier-transform profilometry: a single-shot three-dimensional shape measurement of objects with large height discontinuities and/or surface isolations[J]. *Applied Optics*, 1997, 36(22): 5 347–5 354.

[33] KOLENOVIC E, OSTEN W, KLATTENHOFF R, et al. Miniaturized digital holography sensor for distal three-dimensional endoscopy[J]. *Applied Optics*, 2003, 42(25): 5 167–5 172.

[34] GONG X L, TOYOOKA S. Investigation on mechanism of plastic deformation by digital speckle pattern interferometry[J]. *Experimental Mechanics*, 1999, 39(1): 25–29.

[35] RESTIVO G, CLOUD G L, BEAUDRY R, et al. 3-D Strain fields using embedded DSPI: pilot study[C]//*Proceedings of the 2004 SEM X International Congress and Exposition on Experimental and Applied Mechanics*, 2004: 178–185.

[36] BAIK S H, PARK S K, KIM C J, et al. Two-channel spatial phase shifting electronic speckle pattern interferometer[J]. *Optics Communications*, 2001, 192(3): 205–211.

[37] BURKE J, HELMERS. Performance of spatial vs. temporal phase shifting in ESPI[C]//*Proc. SPIE*, 1999, 3 744(99): 188–199.

[38] BURKE J, HELMERS H, KUNZE C, et al. Speckle intensity and phase gradients: influence on fringe quality in spatial phase shifting ESPI-systems[J]. *Optics Communications*, 1998, 152(1): 144–152.

[39] TAY C J, FU Yu. Determination of curvature and twist by digital shearography and wavelet transforms[J]. *Optics Letters*, 2005, 30(21): 2 873–2 875.

[40] KREIS T. Digital holographic interference-phase measurement using the Fourier-transform method[J]. *Journal of the Optical Society of America A*, 1986, 3(6): 847–855.

[41] HAINES K A, HILDEBRAND B P. Surface-deformation measurement using the wavefront reconstruction technique[J]. *Applied Optics*, 1966, 5(4): 595–602.

[42] FU Yu, Guo Ming, LIU H. Determination of instantaneous curvature and twist by digital shearography[J]. *Optical Engineering*, 2012, 51(8): 083602-1.

[43] PEDRINI G, ZOU Y L, TIZIANI H J. Quantitative evaluation of digital shearing interferogram using the spatial carrier method[J]. *Pure and Applied Optics: Journal of the European Optical Society Part A*, 1999, 5(3): 313.

[44] PEDRINI G, OSTEN W, GUSEV M E. High-speed digital holographic interferometry for vibration measurement[J]. *Applied Optics*, 2006, 45(15): 3 456–3 462.

[45] KOHLER C, VIOTTI M R, ALBERTAZZI G A. Measurement of three-dimensional deformations using digital holography with radial sensitivity[J]. *Applied Optics*, 2010, 49(20): 4 004–4 009.

[46] BHADURI B, MOHAN N K, KOTHIYAL M P. Simultaneous measurement of out-of-plane displacement and slope using a multiaperture DSPI system and fast Fourier transform[J]. *Applied Optics*, 2007, 46(23): 5 680–5 686.

[47] PEDRINI G, Zou Y L, TIZIANI H J. Simultaneous quantitative evaluation of in-plane and out-of-plane deformations by use of a multidirectional spatial carrier[J]. *Applied Optics*, 1997, 36(4): 786–792.

[48] SCHEDIN S, PEDRINI G, TIZIANI H J, et al. Simultaneous three-dimensional dynamic deformation measurements with pulsed digital holography[J]. *Applied Optics*, 1999, 38(34): 7 056–7 062.

[49] BHADURI B, MOHAN N K, KOTHIYAL M P, et al. Use of spatial phase shifting technique in digital speckle pattern interferometry (DSPI) and digital shearography(DS)[J]. *Optics Express*, 2006, 14(24): 11 598–11 607.

[50] XIE Xin, XU Nan, SUN Jianfei, et al. Simultaneous measurement of deformation and the first derivative with spatial phase-shift digital shearography[J]. *Optics Communications*, 2012, 286(1): 277–281.

[51] XIE Xin, YANG L X, XU Nan, et al. Michelson interferometer based spatial phase shift shearography[J]. *Applied Optics*, 2013, 52(17): 4 063–4 071.

[52] FUNG Y C. *A first course in continuum mechanics: for physical and biological engineers and scientists*[M]. Englewood Cliffs, NJ: Prentice-Hall, 1994.

[53] LIU Sheng, THOMAS D, PRAVEEN R, et al. Vibration measurement of MEMS by digital laser microinterferometer[C]//

Proc. SPIE, 2005, 5 878: 103–111.

Biographical notes

YANG Lianxiang received his PhD degree in mechanical engineering from the *University of Kassel*, *Germany*, in 1997. He is the director of optical laboratory and a professor in the department of mechanical engineering at *Oakland University* in USA. Prior to joining *Oakland University* in 2001, he was a R&D scientist at *JDS-Uniphase, Canada*, from 2000 to 2001, a senior engineer at *Dantec-Ettemeyer AG*(currently called *Dantec-Dynamics GmbH*), *Germany*, from 1998 to 2000, a research and senior research fellow at *the University of Kassel, Germany*, from 1991 to 1998, and a lecture at *Hefei University of Technology, China*, from 1986 to 1991. He has multi-disciplinary research experiences including optical metrology, experimental strain/stress analysis, nondestructive testing, and 3D computer vision. He is a fellow of *SPIE*, a Changjiang Scholar of *Hefei University of Technology, China*, and an adjunct professor of *Beijing Information Science &Technology University, China*.

XIE Xin is currently a PhD candidate at *Optical Lab, Oakland University, United State of America.* He received his bachelor of engineering in precise mechanical engineering from *Hefei University of Technology* in 2010 and master of science in mechanical engineering from *Oakland University* in 2012. His main research interests include optical metrology, phase-shift technology, digital shearography, non-destructive testing.

ZHU Lianqing is a professor of *the School of Instruments Science & Optoelectronic Engineering, Beijing Information Science &Technology University, China*. He has multi-disciplinary research experiences including optical metrology, biomedical detection technology and 3D computer vision. He is the director of *Beijing Engineering Research Center of Photoelectric Information and Instruments*, a council member of *Chinese Society for Measurement*, an executive member of the council and assistant secretary general at *Mechanical Quantity Measurement Instrument Federation of China Instrument and Control Society*.

WU Sijin received his PhD degree in optical engineering from *Beijing Jiaotong University, China* in 2012. Prior to receiving his PhD degree, he was an exchanged PhD candidate in *the Optical Laboratory at Oakland University* for two years. He joined *Beijing Information Science & Technology University* in July 2012 as a faculty member. His research interests include optical metrology, such as digital holography and digital shearography, experimental strain/stress analysis, nondestructive testing, 3D computer vision, etc.

WANG Yonghong received his PhD degree in precision mechanical engineering from *Hefei University of Technology, China*, in 2004. He was a postdoctoral fellow in *the optical laboratory at Oakland University* in Michigan from 2007 to 2008. He is currently a professor in *the school of instrument science and opto-electronic engineering, Hefei University of Technology*. He has authored and co-authored over 30 scientific research papers, owned 4 Chinese patents in the areas of optical techniques for whole-field and 3D measurement. His current research interests are precision metrology, advanced optical measuring techniques and image processing and their applications for the automotive, high-tech, and biomedical industries.